Abstracta

Ano XIII - N. 06

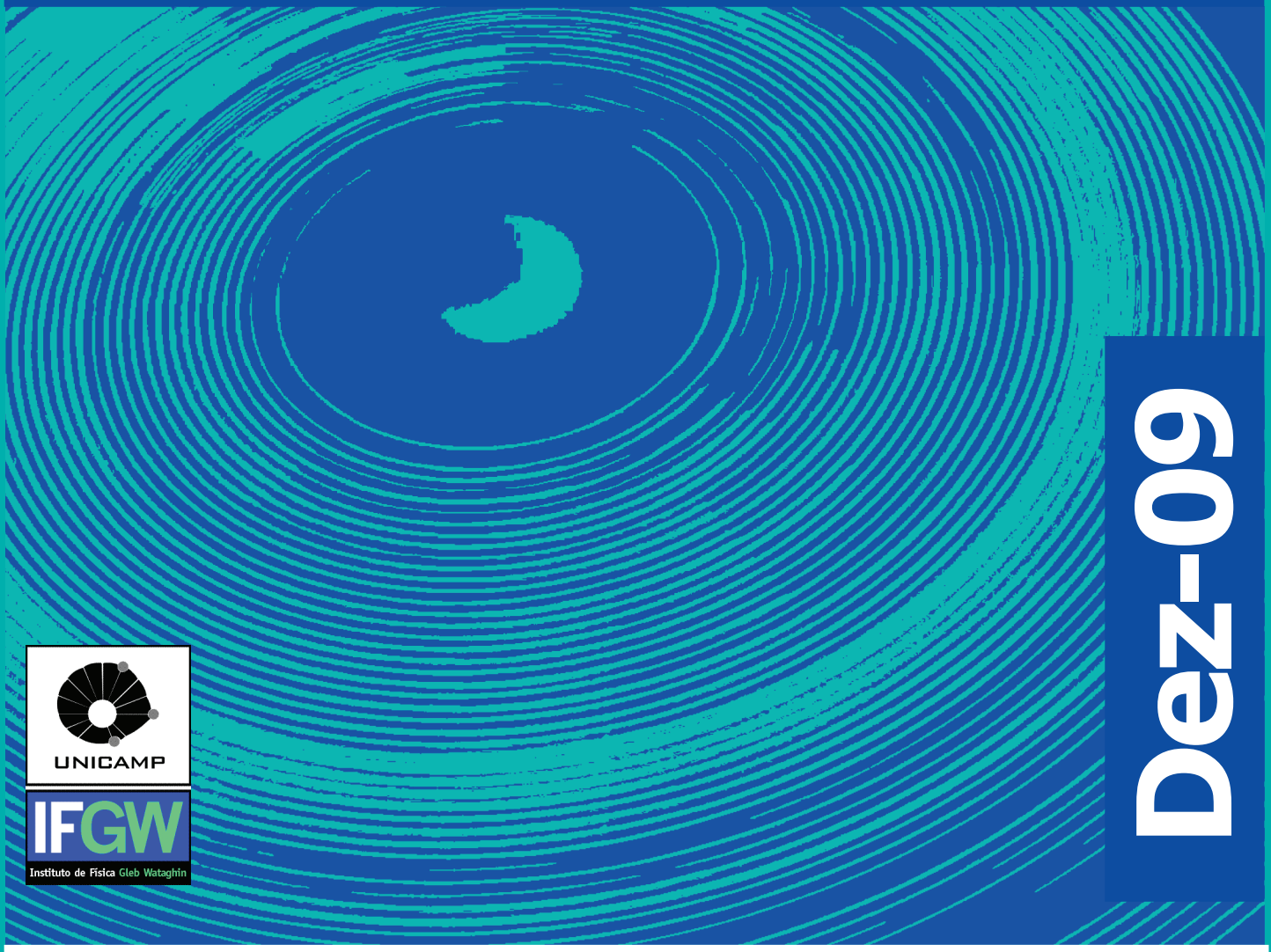

Dez-09

UNICAMP

IFGW

Instituto de Física Gleb Wataghin

Trabalhos Publicados

Novembro 2009 à Dezembro 2009

P204-09 à P254 -09

Trabalhos Publicados

P204-09 "A New Setup for Ground-based Measurements of Solar Activity at 10 mu m (vol 118, pg 1558, 2006)"

Melo, A. M., Marcon, R., Kaufmann, P., Kudaka, A. S., Marun, A., Pereyra, P., Raulin, J. P., and Levato, H.

Publications of the Astronomical Society of the Pacific 121[885], 1296. 2009.

P205-09 "A theoretical study of exciton energy levels in laterally coupled quantum dots"

Barticevic, Z., Pacheco, M., Duque, C. A., and Oliveira, L. E.

A theoretical study of the electronic and optical properties of laterally coupled quantum dots, under applied magnetic fields perpendicular to the plane of the dots, is presented. The exciton energy levels of such laterally coupled quantum-dot systems, together with the corresponding wavefunctions and eigenvalues, are obtained in the effective-mass approximation by using an extended variational approach in which the magnetoexciton states are simultaneously obtained. One achieves the expected limits of one single quantum dot, when the distance between the dots is zero, and of two uncoupled quantum dots, when the distance between the dots is large enough. Moreover, present calculations-with appropriate structural dimensions of the two-dot system-are shown to be in agreement with measurements in self-assembled laterally aligned GaAs quantum-dot pairs and naturally/accidentally occurring coupled quantum dots in GaAs/GaAlAs quantum wells

Journal of Physics-Condensed Matter 21[40]. 405801. 2009.

P206-09 "Abnormal Functional Hippocampal Inter-Connectivity in Patients with Unilateral Mesial Tle Is Worse in Left-Sided Hippocampal Seizure Focus"

Pereira, F., Alessio, A., Rondina, J., Pedro, T., Sercheli, M., Ozelo, H., Bilevicius, E., Zibetti, M., Castellano, G., Covolan, R., Damasceno, B., and Cendes, F.

Epilepsia 50, 16-16. 2009.

P207-09 "Ambipolar diffusion and spatial and time-resolved spectroscopies in semiconductor heterostructures"

Vasconcellos, A. R., Brasil, M. J. S. P., Luzzi, R., Silva, A. A. P., and Leite, A. H. S.

An analysis of the hydrodynamic motion of the fluid of photoinjected carriers in polar semiconductors is presented. Experiments of time-resolved photoluminescence, which provide relevant insights into the dynamical behavior of heterostructures, are analyzed. We study the propagation and recombination of carriers in semiconductor devices with a large cap layer, where carriers are photoinjected, and a quantum well where they recombine. The movement of the photoinjected, and away from equilibrium, carriers along such cap layer consists, to a good degree of approximation, in an ambipolar diffusivelike one, which decays in time as a result of recombination and the coupling, via Coulomb interaction, with the optical and acoustic plasma waves. The density of the electrons arriving at the interface with the quantum well can be determined; these electrons are transferred through the interface to recombine in the quantum well, and the resulting intensity of the time-resolved luminescence is obtained. Comparison with experimental data shows a good agreement. (C) 2009 American Institute of Physics. [DOI: 10.1063/1.3173176]

Journal of Applied Physics 106[4]. 043503. 2009.

P208-09 "An extension of Palumbo's method of solution for the Grad-Shafranov equation"

Hernandesa, J. A. and Clemente, R. A.

We present an extension of Palumbo's method for solving Grad Shafranov equation for ideal axisymmetric magnetohydrodynamic equilibria. The method relies essentially on an expansion in even powers of radius for the square of the gradient of the magnetic stream function and a suitable coordinate transformation that allows reducing the problem of mapping magnetic surface to quadratures. The resulting exact equilibria have magnetic surface contours different from isodynamic ones, allowing modeling flattened or D-shaped plasma tori. (C) 2009 American Institute of Physics. [DOI: 10.1063/1.3208041]

Physics of Plasmas 16[8]. 082509. 2009.

P209-09 "Atmospheric effects on extensive air showers observed with the surface detector of the Pierre Auger observatory"

Abraham, J., Abreu, P., Aglietta, M., Aguirre, C., Ahn, E. J., Allard, D., Allekotte, I., et al

Atmospheric parameters, Such as pressure (P), temperature (T) and density (rho proportional to P/T), affect the development of extensive air showers initiated by energetic cosmic rays. We have Studied the impact of atmospheric variations on extensive air showers by means of the surface detector of the Pierre Auger Observatory. The rate of events shows a similar to 10% seasonal modulation and similar to 2% diurnal one. We find that the observed behaviour is explained by a model including the effects associated with the variations of P and rho. The former affects the longitudinal development of air showers while the latter influences the Moliere radius and hence the lateral distribution of the shower particles. The model is validated with full simulations of extensive air showers using atmospheric profiles measured at the site of the Pierre Auger Observatory. (C) 2009 Elsevier B.V. All rights reserved

Astroparticle Physics 32[2], 89-99. 2009.

P210-09 "Broadband cascaded four-wave mixing by using a three-pump technique in optical fibers"

Cerqueira, S. A., Marconi, J. D., Hernandez-Figueroa, H. E., and Fragnito, H. L.

We present an optimized technique to generate frequency combs by four-wave mixing in highly nonlinear low-dispersion fibers. Three-pumps with unequally spaced frequencies (separation of 100 and 200 GHz) were used. The pumps were located relatively close to the zero-dispersion wavelength of the fiber. Using this three-pump technique we obtained a total of 275 FWM products experimentally, with a 100 GHz spacing and a spanning of over 220 nm. (c) 2009 Elsevier B.V. All rights reserved

Optics Communications 282[22], 4436-4439. 2009.

P211-09 "Construction of white-light holographic screens"

Lunazzi, J. J., Magalhaes, D. S. F., and Serra, R. L.

We describe one setup employed for the recording of two types of holographic screens that can be used in white-light

applications. We show how to obtain holographic screens with areas up to 1370 cm(2) and diffraction efficiency of 17%. We analyze the holographic screens in their relevant aspects as to focal lengths, theoretical approach, sizes, and diffraction efficiencies, specifying when each type is appropriate for particular applications. (C) 2009 Society of Photo-Optical Instrumentation Engineers. [DOI: 10.1117/1.3231503]

Optical Engineering 48[9]. 095802. 2009.

P212-09 "Doping effects on the magnetic properties of NdRhIn5 intermetallic antiferromagnet"

Lora-Serrano, R., Garcia, D. J., Miranda, E., Adriano, C., Bufaical, L., Duque, J. G. S., and Pagliuso, P. G.

We report temperature dependent heat capacity and magnetization measurements on single crystals of Nd1-xLaxRhIn5 (x = 0.15, 0.4 and 0.5) and NdRhIn5-xSnx (x = 0.08, 0.12 and 0.24). NdRhIn5 is an antiferromagnetic (AFM) compound with T-N approximate to 11 K which crystallizes in the same layered tetragonal structure of the CeMIn5 family (M = Rh, Co and Ir), where different ground states can be found by tuning the interplay among different microscopic interactions such as the Kondo effect, crystal field (CEF) effects and the Ruderman-Kittel-Kasuya-Yoshida (RKKY) magnetic interaction. Here, we explore the evolution of the AFM correlations in this Nd-based (non-Kondo) compound while perturbing the RKKY exchange by using two different substitutions: (i) replacing Nd3+ by non-magnetic La3+ within NdIn3 atomic planes (dilution) and (ii) substituting In by Sn in the In-sites (electronic tuning). For both types of doping, our results show the suppression of the AFM state as the La- or Sn-content is increased. This doping induced suppression of the AFM order is discussed considering the effects of dilution and effects in the tetragonal CEF using a mean-field model applied to the observed data. Our results are compared to the properties of other members of the RRhIn5 family considering the role of dimensionality in the magnetic interactions. (C) 2009 Elsevier B.V. All rights reserved

Physica B-Condensed Matter 404[19], 3059-3062. 2009.

P213-09 "Effective quantum dynamics of two Brownian particles"

Duarte, O. S. and Caldeira, A. O.

We use the system-plus-reservoir approach to study the quantum dynamics of a bipartite continuous variable system (two generic particles). We present an extension of the traditional model of a bath of oscillators which is capable of inducing an effective coupling between the two parts of the system depending on the choice made for the spectral density of the bath. The coupling is nonlinear in the system variables and an exponential dependence on these variables is imposed in order to guarantee the translational invariance of the model if the two particles are not subject to any external potential. The reduced density operator is obtained by the functional integral method. The dynamical susceptibility of the reservoir is modeled in order to introduce, besides a characteristic frequency, a characteristic length that determines if the effective interaction potential is strong enough to induce entanglement between the particles. Our model provides a criterion of distance for identifying in which cases a common environment can induce entanglement. Three regimes are found: the short distance regime, equivalent to a bilinear system-reservoir coupling, the long distance regime in which the particles act like coupled to independent reservoirs, and the intermediate regime suitable for the competition between decoherence and induced entanglement

Physical Review A 80[3]. 032110. 2009.

P214-09 "Effects of Ga+ milling on InGaAsP quantum well laser with mirrors milled by focused ion beam"

Vallini, F., Figueira, D. S. L., Jarschel, P. F., Barea, L. A. M., Von Zuben, A. A. G., and Frateschi, N. C.

InGaAsP/InP quantum well ridge waveguide lasers were fabricated for the evaluation of Ga+ focused ion beam milling of mirrors. Electrical and optical properties were investigated. A 7% increment in the threshold current, a 17% reduction in the external quantum efficiency, and a 15 nm blueshift in the emission spectrum were observed after milling as compared to the as-cleaved facet result. Annealing in inert atmosphere partially reverts these effects, resulting in a 4% increment in the threshold current, an 11% reduction in the external efficiency, and a 13 nm blueshift with the as-cleaved result. The current-voltage behavior after milling and annealing shows a very small increase in leakage current, indicating that optical damage is the main effect of the milling process. (C) 2009 American Vacuum Society. [DOI:10.1116/1.3207741]

Journal of Vacuum Science & Technology B 27[5], L25-L27. 2009.

P215-09 "Electron spin resonance of Gd3+ in the antiferromagnetic heavy fermion CeIn3 and its reference compound LaIn3"

Bittar, E. M., Duque, J. G. S., Venegas, P. A., Rettori, C., and Pagliuso, P. G.

Wereport temperature dependent electron spin resonance (ESR) experiments of Gd3+ in CeIn3 and in its reference compound LaIn3 taken in crushed single crystals. For LaIn3 a single Dysonian Gd3+ ESR line with a nearly temperature independent g similar to 2.020(5) is observed, and its linewidth follows a Korringa-like behavior as a function of temperature. From the Korringa rate (Delta H/Delta T similar to 16 Oe/K) and g-shift (Delta g similar to 0.027) we have extracted the exchange parameter between the Gd3+ local moments and the conduction electrons (ce) in this compound. This exchange parameter J(fs) approximate to 20 meV was found to be ce wave-vector independent. For CeIn3, the Gd3+ ESR spectra were found to be weakly temperature dependent and present partly resolved Gd3+ fine-structure. Interestingly, for CeIn3, the g-shift with respect to the g-value of Gd3+ in insulators is negative, in contrast to the positive g-shift found for Gd3+ in LaIn3. These results suggests different electronic structure at the Gd3+ site in the Kondo antiferromagnet host CeIn3. Possibly, Kondo effect may cause a decrease of the s-like conduction electron density of states at the Gd3+ site, giving arise to an exchange interaction only between the Gd3+ local moment and the Ce 4f electrons. (C) 2009 Elsevier B.V. All rights reserved

Physica B-Condensed Matter 404[19], 2995-2998. 2009.

P216-09 "Electron spin resonance (ESR) of Eu2+ in type-I clathrate Eu8Ga16Ge30"Holanda, L. M., Vargas, J. M., Rettori, C., Pagliuso, P. G., Bittar, E. M., Avila, M. A., and Takabatake, T.

We report temperature dependent X-band (nu similar to 9.5 GHz) electron spin resonance (ESR) experiments in type-I clathrate Eu8Ga16Ge30. This system presents interesting thermoelectric properties in its paramagnetic state and orders ferromagnetically below T-C = 35 K Although the Eu2+ ions sits on two inequivalent sites in the type-I clathrate structure, we found in the paramagnetic state a single Dysonian Eu2+ ESR line with a nearly temperature independent g similar to 2 is observed, and its linewidth follows a Korringa-like behavior as a function of temperature. The microscopic details of the exchange coupling between the Eu2+ local moments and the conduction-electrons (c-e) in this compound are investigated through the obtained Korringa rate (Delta H/Delta T similar to 1 (1) Oe/K) and g-shift (Delta g similar to 0.01(1)) from ESR experiments combined with the magnetic susceptibility and specific heat data. (c) 2009 Elsevier B.V. All rights reserved

***Physica B-Condensed Matter* 404[19], 3300-3303. 2009.**

P217-09 "Energy-resolved spatial inhomogeneity of disordered Mott systems"

Andrade, E. C., Miranda, E., and Dobrosavljevic, V.

We investigate the effects of weak to moderate disorder on the T = 0 Mott metal-insulator transition in two dimensions. Our model calculations demonstrate that the electronic states close to the Fermi energy become more spatially homogeneous in the critical region. Remarkably, the higher energy states show the opposite behavior: they display enhanced spatial inhomogeneity precisely in the close vicinity to the Mott transition. We suggest that such energy-resolved disorder screening is a generic property of disordered Mott systems. (C) 2009 Elsevier B.V. All rights reserved

Physica B-Condensed Matter 404[19], 3167-3171. 2009.

P218-09 "ESR determination of the crystal field parameters of Nd, Dy, Er, and Yb doped skutterudite CeFe4P12"

Garcia, F. A., Garcia, D. J., Duque, J. G. S., Pagliuso, P. G., Rettori, C., Schlottmann, P., Torikachvili, M. S., and Oseroff, S. B.

Despite extensive research on the skutterudites for the last decade, their electric crystalline field ground state is still a matter of controversy. By using electron spin resonance measurements we show that an appropriate description of the ground state can be given for the T-h cubic symmetry of the Ce1-xRxFe4P12 (R = Dy, Er, Yb, x less than or similar to 0.003) skutterudite compounds. From the analysis of the ESR data the three crystal field parameters, B-4(c), B-6(c) and B-6(t) were determined for each of these rare-earths at the Ce3+ site. (c) 2009 Elsevier B.V. All rights reserved

Physica B-Condensed Matter 404[19], 3281-3284. 2009.

P219-09 "Evidence for a subtle structural symmetry breaking in EuB6"

Martinho, H., Rettori, C., Dalpian, G. M., da Silva, J. L. F., Fisk, Z., and Oseroff, S. B.

This work presents a systematic Raman scattering study and first-principles calculations for the EuB6 system. Evidence for the presence of an incipient (similar to 1x10(-4) angstrom) tetragonal symmetry break of its crystalline structure was found. Forbidden Raman modes at omega(fRm(1)) similar to 1170 cm(-1), omega(fRm(2)) similar to 1400 cm(-1), and omega(fRm(3)) similar to 1500 cm(-1) were observed. The tetragonal symmetry of omega(fRm(2)) and omega(fRm(3)) together with spin-polarized first-principles simulations of the structural and magnetic properties fully support such a break of symmetry. Our data and calculations explain the occurrence of ferromagnetism in Eu hexaborides, previously reported

Journal of Physics-Condensed Matter 21[45]. 456007. 2009.

P220-09 "Evidence of space charge regions within semiconductor nanowires from Kelvin probe force microscopy"

Narvaez, A. C., Chiaramonte, T., Vicaro, K. O., Clerici, J. H., and Cotta, M. A.

We have studied the equilibrium electrostatic profile of III-V semiconductor nanowires using Kelvin probe force microscopy. Qualitative agreement of the measured surface potential levels and expected Fermi level variation for pure InP and InAs nanowires is obtained from electrical images with spatial resolution as low as 10 nm. Surface potential mapping for pure and heterostructured nanowires suggests the existence of charge transfer mechanisms and the formation of a metal-semiconductor electrical contact at the nanowire apex

Nanotechnology 20[46]. 465705. 2009.

P221-09 "Fabrication, structural and magnetic characterization of thin microwires with novel composition Cu-70(Co70Fe5Si10B15)(30)"

Garcia, C., Zhukov, A., Gonzalez, J., del Val, J. J., Blanco, J. M., Knobel, M., and Zhukova, V.

We report on fabrication, structural and magnetic characterization Of Cu-70(Co70Fe5Si10B15)(30) microwires with total diameter of 28.2 mu m and metallic nucleus diameter of 15.2 mu m produced by the Taylor-Ulitovski method containing 30% of alloy composition commonly used amorphous soft magnetic material and 70% Cu. The structure consists of crystalline Cu, and mixture of ferromagnetic phases. The as-prepared Cu-70(Co70Fe5Si10B15)(30) microwires present coercivity of about 85 Oe at room temperature. Temperature dependence of coercivity is measured. Significant increase of coercivity till 135 Oe is observed at about 50 K Magnetization measured under applied magnetic field (FC) and without magnetic field (ZFC) exhibit significant difference attributed to the inhomogeneity of as-prepared samples consisting of crystalline paramagnetic Cu matrix with ferromagnetic entities. MR related with existence of ferromagnetic grains in paramagnetic Cu matrix has been observed. This MR increases with decreasing temperature (up to 1.6% at 5 K). (C) 2008 Elsevier B.V. All rights reserved

Journal of Alloys and Compounds 483[1-2], 566-569. 2009.

P222-09 "Field-dependent collective ESR mode in YbRh2Si2"

Holanda, L. M., Duque, J. G. S., Bittar, E. M., Adriano, C., Pagliuso, P. G., Rettori, C., Hu, R. W., Petrovic, C., Maquilon, S., Fisk, Z., Huber, D. L., and Oseroff, S. B.

Electron spin resonance (ESR) experiments in YbRh2Si2 Kondo lattice (T-K similar or equal to 25 K) at different field/frequencies (4.1 <= v <= 34.4 GHz) and H-perpendicular to c revealed: (i) a strong field dependent Yb3+ spin-lattice relaxation, (ii) a weak field and T-dependent effective g-value, (iii) a suppression of the ESR intensity beyond 15% of Lu-doping, and (iv) a strong sample and Lu-doping (<= 15%) dependence of the ESR data. These results suggest that the ESR signal in YbRh2Si2 may be due to a coupled Yb3+-conduction electron resonant collective mode with a subtle field-dependent spins dynamic. (C) 2009 Elsevier B.V. All rights reserved

Physica B-Condensed Matter 404[19], 2964-2968. 2009.

P223-09 "Functional and small-angle X-ray scattering studies of a new stationary phase survival protein E (SurE) from Xylella fastidiosa - evidence of allosteric behaviour"

Saraiva, A. M., Reis, M. A., Tada, S. F., Rosselli-Murai, L. K., Schneider, D. R. S., Pelloso, A. C., Toledo, M. A. S., Giles, C., Aparicio, R., and de Souza, A. P.

The genome data of bacterium Xylella fastidiosa strain 9a5c has identified several orfs related to its phytopathogenic adaptation and survival. Among these genes, the surE codifies a survival protein E (XfSurE) whose function is not so well understood, but functional assays in Escherichia coli revealed nucleotidase and exopolyphosphate activity. In the present study, we report the XfSurE protein overexpression in E. coli

and its purification. The overall secondary structure was analyzed by CD. Small-angle X-ray scattering and gel. filtration techniques demonstrated that the oligomeric state of the protein in solution is a tetramer. In addition, functional kinetics experiments were carried out with several monophosphate nucleoside substrates and revealed a highly positive cooperativity. An allosteric mechanism involving torsion movements in solution is proposed to explain the cooperative behaviour of XfSurE. This is the. first characterization of a SurE enzyme from a phytopathogen organism and, to our knowledge, the. first solution structure of a SurE protein to be described

Febs Journal 276[22], 6751-6762. 2009.

P224-09 "Graphene to graphane: a theoretical study"

Flores, M. Z. S., Autreto, P. A. S., Legoas, S. B., and Galvao,D.S.

Graphane is a two-dimensional system consisting of a single layer of fully saturated (sp(3) hybridization) carbon atoms. In an ideal graphane structure C-H bonds exhibit an alternating pattern (up and down with relation to the plane defined by the carbon atoms). In this work we have investigated, using ab initio and reactive molecular dynamics simulations, the role of H frustration (breaking the H atoms' up and down alternating pattern) in graphane-like structures. Our results show that a significant percentage of uncorrelated H frustrated domains are formed in the early stages of the hydrogenation process leading to membrane shrinkage and extensive membrane corrugations. These results also suggest that large domains of perfect graphane-like structures are unlikely to be formed, as H frustrated domains are always present

Nanotechnology 20[46]. 465704. 2009.

P225-09 "Growth of Long Range Forward-Backward Multiplicity Correlations with Centrality in Au plus Au Collisions at root s(NN)=200 GeV"

Abelev, B. I., Aggarwal, M. M., Ahammed, Z., Anderson, B. D., Arkhipkin, D., Averichev, G. S., Balewski, et all

Forward-backward multiplicity correlation strengths have been measured with the STAR detector for Au + Au and p + p collisions at root s(NN) = 200 GeV. Strong short- and long-range correlations (LRC) are seen in central Au + Au collisions. The magnitude of these correlations decrease with decreasing centrality until only short-range correlations are observed in peripheral Au + Au collisions. Both the dual parton model (DPM) and the color glass condensate (CGC) predict the existence of the long-range correlations. In the DPM, the fluctuation in the number of elementary (parton) inelastic collisions produces the LRC. In the CGC, longitudinal color flux tubes generate the LRC. The data are in qualitative agreement with the predictions of the DPM and indicate the presence of multiple parton interactions

Physical Review Letters 103[17]. 172301. 2009.

P226-09 "In vitro and in vivo documentation of quantum dots labeled Trypanosoma cruzi-Rhodnius prolixus interaction using confocal microscopy"

Feder, D., Gomes, S. A. O., de Thomaz, A. A., Almeida, D. B., Faustino, W. M., Fontes, A., Stahl, C. V., Santos-Mallet, J. R., and Cesar, C. L.

Semiconductor quantum dots (QDs) are highly fluorescent nanocrystals markers that allow long photobleaching and do not destroy the parasites. In this paper, we used fluorescent core shell quantum dots to perform studies of live parasite-vector interaction processes without any observable effect on the vitality of parasites. These nanocrystals were synthesized in aqueous medium and physiological pH, which is very important for monitoring live cells activities, and conjugated with molecules such as lectins to label specific carbohydrates involved on the parasite-vector interaction. These QDs were successfully used for the study of in vitro and in vivo interaction of Trypanosoma cruzi and the triatomine Rhodnius prolixus. These QDs allowed us to acquire real time confocal images sequences of live T. cruzi-R. prolixus interactions for an extended period, causing no damage to the cells. By zooming to the region of interest, we have been able to acquire confocal images at the three to four frames per second rate. Our results show that QDs are physiological fluorescent markers capable to label living parasites and insect vector cells. QDs can be functionalized with lectins to specifically mark surface carbohydrates on perimicrovillar membrane of R. prolixus to follow, visualize, and understand interaction between vectors and its parasites in real-time

Parasitology Research 106[1], 85-93. 2009.

P227-09 "Inelastic X-ray scattering and first-principles study of electron excitations in MgB2"

Stutz, G., Silkin, V. M., Tirao, G., Balassis, A., Chulkov, E. V., Echenique, P. M., Granado, E., Garcia-Flores, A. F., and Pagliuso, P. G.

An experimental and theoretical study of electronic excitations in MgB2 covering the domain of large energy and momentum transfers is reported. Energy-loss spectra for several values of momentum transfers were measured in a polycrystalline sample by means of inelastic X-ray scattering spectroscopy. Ab initio calculations of the dielectric function as well as the energy-loss function were performed in the frame of the time-dependent local density approximation with inclusion of crystal local-field effects. We obtained very good agreement between the experimental and the theoretical energy dispersion of the peak maximum of the loss function. We found that crystal local-field effects are responsible for this agreement at large momenta. Fine structure observed in the measured spectra was interpreted in terms of strong interband transitions predicted by the calculations in the Gamma A and Gamma K directions. The theoretical dispersion of these features is in good accordance with the experimental data. Further spectral features in the measured spectra due to Mg 2s and 2p core electron excitations are also discussed. (c) 2009 Elsevier Ltd. All rights reserved

Solid State Communications 149[39-40], 1706-1711. 2009.

P228-09 "Interplay between crystallization and particle growth during the isothermal annealing of colloidal iron oxide nanoparticles"

Haddad, P. S., Rocha, T. R., Souza, E. A., Martins, T. M., Knobel, M., and Zanchet, D.

The relationship between crystallization and growth of colloidal iron oxide nanoparticles during isothermal annealing was addressed in this work. The structural, morphological and chemical modifications of the nanoparticles during thermal treatments were followed by combination of electron microscopy, X-ray diffraction and spectroscopic methods. The initially monodisperse spherical nanoparticles with amorphous and partially oxidized structure evolved during the treatments, depending on the temperature and treatment time. Core-void-shell nanoparticles or single crystal nanoparticles and hollow polycrystalline nanoparticles, both with well defined Fe3O4 oxide phase, are formed depending on the conditions. This evolution was interpreted as a result of the Kirkendall effect associated to mass redistribution and fragmentation of the nanoparticles, bringing new information about the effect of post-synthesis treatments on the crystallinity and morphology of colloidal nanoparticles. (C) 2009 Elsevier Inc. All rights reserved

Journal of Colloid and Interface Science 339[2], 344-350. 2009.

P229-09 "J/psi production at high transverse momenta in p plus p and Cu plus Cu collisions at root s(NN)=200 GeV"

Abelev, B. I., Aggarwal, M. M., Ahammed, Z., Anderson, B. D., Arkhipkin, D., Averichev, G. S., Balewski, et all

The STAR Collaboration at the Relativistic Heavy Ion Collider presents measurements of J/psi e(+) e(-) at midrapidity and high transverse momentum (pT > 5 GeV/c) in p + p and central Cu + Cu collisions at root s(NN) = 200 GeV. The inclusive J/psi production cross section for Cu + Cu collisions is found to be consistent at high p(T) with the binary collision-scaled cross section for p + p collisions. At a confidence level of 97%, this is in contrast to a suppression of J/psi production observed at lower p(T). Azimuthal correlations of J/psi with charged hadrons in p + p collisions provide an estimate of the contribution of B-hadron decays to J/psi production of 13% +/- 5%

Physical Review C 80[4]. 041902. 2009.

P230-09 "Low-resolution structural studies of human Stanniocalcin-I"

Trindade, D. M., Silva, J. C., Navarro, M. S., Torriani, I. C. L., and Kobarg, J.

Background: Stanniocalcins (STCs) represent small glycoprotein hormones, found in all vertebrates, which have been functionally implicated in Calcium homeostasis. However, recent data from mammalian systems indicated that they may be also involved in embryogenesis, tumorigenesis and in the context of the latter especially in angiogenesis. Human STCI is a 247 amino acids protein with a predicted molecular mass of 27 kDa, but preliminary data suggested its di- or multimerization. The latter in conjunction with alternative splicing and/or post-translational modification gives rise to forms described as STC50 and "big STC", which molecular weights range from 56 to 135 kDa. Results: In this study we performed a biochemical and structural analysis of STCI with the aim of obtaining low resolution structural information about the human STCI, since structural information in this protein family is scarce. We expressed STCI in both E. coli and insect cells using the baculo virus system with a C-terminal 6 x His fusion tag. From the latter we obtained reasonable amounts of soluble protein. Circular dichroism analysis showed STCI as a well structured protein with 52% of alpha-helical content. Mass spectroscopy analysis of the recombinant protein allowed to assign the five intramolecular disulfide bridges as well as the dimerization Cys202, thereby confirming the conservation of the disulfide pattern previously described for fish STCI. SAXS data also clearly demonstrated that STCI adopts a dimeric, slightly elongated structure in solution. Conclusion: Our data reveal the first low resolution, structural information for human STCI. Theoretical predictions and circular dichroism spectroscopy both suggested that STCI has a high content of alpha-helices and SAXS experiments revealed that STCI is a dimer of slightly elongated shape in solution. The dimerization was confirmed by mass spectrometry as was the highly conserved disulfide pattern, which is identical to that found in fish STCI

Bmc Structural Biology 9. 57. 2009.

P231-09 "Low-temperature gas and pressure sensor based on multi-wall carbon nanotubes decorated with Ti nanoparticles"

Gelamo, R. V., Rouxinol, F. P., Verissimo, C., Vaz, A. R., de Moraes, M. A. B., and Moshkalev, S. A.

Multi-wall carbon nanotubes decorated by Ti nanoparticles were used for gas (N-2, Ar, O-2) sensing at low temperatures. Chemiresistor sensor configurations with supported and suspended nanotubes were tested. Two gas sensing mechanisms (chemical and electrothermal) were demonstrated, with their relative contributions strongly depending on the sensor configuration. For suspended nanotubes, heating by Joule effect results in strong enhancement of chemical sensitivity to oxygen. (C) 2009 Elsevier B. V. All rights reserved

Chemical Physics Letters 482[4-6], 302-306. 2009.

P232-09 "Low temperature magnetism of Cd-doped Ce2RhIn8 heavy fermion antiferromagnet"

Adriano, C., Giles, C., Mendonca-Ferreira, L., de Bergevin, F., Mazzoli, C., Paolasini, L., Fisk, Z., and Pagliuso, P. G.

We report the low temperature magnetic properties of Cd-doped single crystals of Ce2RhIn8 grown from In-flux. Measurements of temperature-dependent magnetic susceptibility, heat capacity, electrical resistivity and X-ray magnetic scattering revealed that Cd-doping enhances the antiferromagnetic ordering temperature from T-N = 2.8 to 4.8 K for crystals with nominal Cd-concentration of similar to 20%. Similarly to the pure compound, Cd-doped Ce2RhIn8 presents just below TN a commensurate anti ferro magnetic structure with a propagation vector (eta) over right arrow = (1/2, 1/2, 0). Comparisons between our results and the general effects of Cd-doping on the single layer related family CeMIn5 (M = Co, Rh and Ir) will also be given. (C) 2009 Elsevier B.V. All rights reserved

Physica B-Condensed Matter 404[19], 3014-3017. 2009.

P233-09 "Magnetic properties of (Ce1-xLax)PdIn2"

da Silva, L. M., dos Santos, A. O., de Melo, M. C., Cardoso, L. P., Medina, A. N., and Gandra, F. G.

We report on results of X-ray powder diffraction, magnetization and specific heat measurements of the pseudo-ternary (Ce1-xLax)PdIn2 system with x = 0; 0.2; 0.4 and 0.6. The results show a linear increase of the unit cell volume and a reduction of the ferromagnetic transition as La content increases. The Debye temperature, Sommerfeld coefficient and crystal field parameters were estimated from specific heat data, and are found to be weakly dependent of the Ce concentration. Also, the variation of magnetic entropy at T-C is only weakly dependent on x (Delta S congruent to 0.92RIn(2)) indicating that T-K/T-C is approximately constant along the series. The T-C and T-K behaviors are explained by the variation of the exchange parameter due to the volume change when Ce is replaced by La. Our results indicate that the chemical pressure is the dominant effect rather than the chemical disorder for determining the physical proprieties of the (Ce1-xLax)PdIn2 system. (C) 2009 Elsevier B.V. All rights reserved

Physica B-Condensed Matter 404[19], 3018-3020. 2009.

P234-09 "Magnetic structure of Ho2CoGa8 determined by X-ray resonant magnetic scattering"

Adriano, C., Giles, C., Coelho, L. N., Faria, G. A., and Pagliuso, P. G.

We report the low temperature magnetic structure of the Ho2CoGa8 intermetallic compound studied by X-ray magnetic scattering technique at the Brazilian Synchrotron Light Laboratory. We found that below T-N = 5.1 K Ho2CoGa8 has a commensurate antiferromagnetic structure with a propagation vector (eta) over bar = (1/2, 1/2, 1/2) and preliminary analysis indicated that the Ho magnetic moment points along the c-axis. The magnetic structure of this compound was obtained by measuring the strong dipolar resonant peak at the L-3 edge using polarization analysis. The magnetic structure and properties Ho2CoGa8 are found to be consistent with the general trend already seen for the Nd-, Tb-, and the Ce-based compounds from the RmMnIn3m+2n family (R = rare earth; M =

Co, Rh, or Ir; m = 1,2: n = 0, 1). (c) 2009 Elsevier B.V. All rights reserved

Physica B-Condensed Matter 404[19], 3289-3292. 2009.

P235-09 "Molecular-dynamics simulation of threshold displacement energies in zircon"

Moreira, P. A. F. P., Devanathan, R., Yu, J. G., and Weber, W. J.

Molecular-dynamics simulations were used to examine the displacement threshold energy (E-d) surface for Zr, Si and O in zircon using two different interatomic potentials. For each sublattice, the simulation was repeated from different initial conditions to estimate the uncertainty in the calculated value of E-d. The displacement threshold energies vary considerably with crystallographic direction and sublattice. Based on the present simulations and previous experimental studies, this work recommends E-d values of 75, 75 and 60 eV for Zr, Si and O, respectively. to be used in Monte Carlo simulations of irradiation damage profile in zircon. (C) 2009 Elsevier B.V. All rights reserved

Nuclear Instruments & Methods in Physics Research Section B-Beam Interactions with Materials and Atoms 267[20], 3431-3436. 2009.

P236-09 "Neutral pion production in Au plus Au collisions at root s(NN)=200 GeV"

Abelev, B. I., Aggarwal, M. M., Ahammed, Z., Alakhverdyants, A. V., Anderson, B. D., Arkhipkin, D.Averichev, G. S.,et all

The results of midrapidity ($0 < y < 0.8$) neutral pion spectra over an extended transverse momentum range ($1 < p(T) < 12$ GeV/c) in root s(NN) = 200 GeV Au + Au collisions, measured by the STAR experiment, are presented. The neutral pions are reconstructed from photons measured either by the STAR Barrel Electro-Magnetic Calorimeter or by the Time Projection Chamber via tracking of conversion electron-positron pairs. Our measurements are compared to previously published pi(+/-) and pi(0) results. The nuclear modification factors R-CP and R-AA of pi(0) are also presented as a function of p(T). In the most central Au + Au collisions, the binary collision scaled pi(0) yield at high p(T) is suppressed by a factor of about 5 compared to the expectation from the yield of p + p collisions. Such a large suppression is in agreement with previous observations for light quark mesons and is consistent with the scenario that partons suffer considerable energy loss in the dense medium formed in central nucleus-nucleus collisions at the Relativistic Heavy Ion Collider

Physical Review C 80[4]. 044905. 2009.

P237-09 "Optical properties in complex-structured nanometric quantum wells: Photoluminescence, photoluminescence excitation, and Stokes shift"

Silva, A. A. P., Vasconcellos, A. R., Luzzi, R., Meneses, E. A., and Laureto, E.

Systems in which one or more directions are in the nanometric space scale exhibit significantly some peculiar phenomena and processes. We consider here the case of nanometric quantum wells with complex structure, displaying fractal-like characteristics, which are part of semiconductor heterostructures. An extensive theoretical study of the optical properties of photoluminescence and excited photoluminescence, and then involving absorption and the question of emergence of the so-called Stokes shift that is observed in some cases are performed. The results are compared with some experimental data. This is of relevance for opening up the possibility to use optical measurements to perform a (nondestructive) quality control of samples grown under different methods and protocols.

(C) 2009 American Institute of Physics. [doi:10.1063/1.3245385]

Journal of Applied Physics 106[8]. 083521. 2009.

P238-09 "Optical properties of III-nitrides in electric fields"

Rodrigues, C. G., Vasconcellos, A. R., and Luzzi, R.

The influence of intermediate to high electric fields on the optical properties of direct-gap strongly-polar III-Nitrides is characterized. It is manifested through the dependence on the electric field of the nonequilibrium thermodynamic state of the system, which is characterized by a nonequilibrium effective temperature (quasi-temperature), quasi-chemical potentials and drift velocities of the excited carriers driven away from equilibrium, and the quasi-temperatures of the phonons in the different branches. In particular, we analyze the processes of absorption and luminescence, and a field-dependent Roosbroeck-Shockley relation is derived. It is shown that it is possible to measure the carriers' drift velocity and quasi-temperature, in the steady state or with ultrafast time resolution, resorting to luminescence together with Raman scattering experiments

European Physical Journal B 72[1], 67-75. 2009.

P239-09 "Plasmon polaritons in photonic superlattices containing a left-handed material"

Reyes-Gomez, E., Mogilevtsev, D., Cavalcanti, S. B., de Carvalho, C. A. A., and Oliveira, L. E.

We analyze one-dimensional photonic superlattices which alternate layers of air and a left-handed material. We assume Drude-type dispersive responses for the dielectric permittivity and magnetic permeability of the left-handed material. Maxwell's equations and the transfer-matrix technique are used to derive the dispersion relation and transmission spectra for the propagation of obliquely incident optical fields. The photonic dispersion indicates that the growth direction component of the electric (or magnetic) field leads to the propagation of electric (or magnetic) plasmon polaritons, for either TE or TM configurations. Furthermore, we show that if the plasma frequency is chosen within the photonic $< n(w) > = 0$ zeroth-order bandgap, the coupling of light with plasmons weakens considerably. As light propagation is forbidden in that particular frequency region, the plasmon-polariton mode reduces to a pure plasmon mode. Copyright (c) EPLA, 2009

Epl 88[2]. 24002. 2009.

P240-09 "Possible scenario for MaVaN's as the only neutrino flavor conversion mechanism in the Sun"

de Holanda, P. C.

Mass Varying neutrino mechanisms were proposed to link the neutrino mass scale with dark energy, addressing the coincidence problem. In some scenarios this mass can present a dependence on the baryonic density felt by neutrinos, creating an effective neutrino mass that depends both on the neutrino and baryonic densities. In this article we investigate the possibility that a neutrino effective mass in matter in addition to a very small mass squared difference in vacuum (O(10(-9) eV(2))) are the main flavour conversion mechanism acting in neutrino oscillation experiments. We present a parameterization on the environmental effects on neutrino mass that produces the right flavour conversion probabilities for solar and terrestrial neutrinos experiments

Journal of Cosmology and Astroparticle Physics [7]. 024. 2009.

P241-09 "Preparation of supported Pt(0) nanoparticles as efficient recyclable catalysts for hydrogenation of alkenes and ketones"

Jacinto, M. J., Landers, R., and Rossi, L. M.

A magnetically recoverable Pt(0) catalyst was prepared by in situ H-2 reduction of Pt2+ species bound to an amino modified silica-coated magnetic nanoparticles. Compared to ordinary silica (maximum uptake Pt 0.03 wt%), the amino-functionalized silica surfaces were loaded with 1.95 wt% of metal. The supported Pt(0) nanoparticles exhibit high catalytic activity in the hydrogenation of alkenes and ketones under solventless mild reaction conditions. Partially hydrogenated products could also be isolated. The magnetic property of the catalyst grants a fast and efficient product isolation compared to traditional methods used in heterogeneous systems that generally make use of time- and solvent-consuming procedures. (C) 2009 Elsevier B.V. All rights reserved

Catalysis Communications 10[15], 1971-1974. 2009.

P242-09 "Probing Individual Quantum Dots: Noise in Self-Assembled Systems"

Vicaro, K. O., Gutierrez, H. R., Seabra, A. C., Schulz, P. A., and Cotta, M. A.

In this work we explore the noise characteristics in lithographically-defined two terminal devices containing self-assembled InAs/InP quantum dots. The experimental ensemble of InAs dots show random telegraph noise (RTN) with tuneable relative amplitude-up to 150%-in well defined temperature and source-drain applied voltage ranges. Our numerical simulation indicates that the RTN signature correlates with a very low number of quantum dots acting as effective charge storage centres in the structure for a given applied voltage. The modulation in relative amplitude variation can thus be associated to the altered electrostatic potential profile around such centres and enhanced carrier scattering provided by a charged dot

Journal of Nanoscience and Nanotechnology 9[11], 6390-6395. 2009.

P243-09 "Quantum confinement and magnetic-field effects on the electron g factor in GaAs-(Ga, Al) As cylindrical quantum dots"

Mejia-Salazar, J. R., Porras-Montenegro, N., and Oliveira, L. E.

We have performed a theoretical study of the quantum confinement (geometrical and barrier potential confinements) and axis-parallel applied magnetic-field effects on the conduction-electron effective Lande g factor in GaAs-(Ga,Al) As cylindrical quantum dots. Numerical calculations of the g factor are performed by using the Ogg-McCombe effective Hamiltonian-which includes non-parabolicity and anisotropy effects-for the conduction-band electrons. The quantum dot is assumed to consist of a finite-length cylinder of GaAs surrounded by a Ga1-xAlxAs barrier. Theoretical results are given as functions of the Al concentration in the Ga1-xAlxAs barrier, radius, lengths and applied magnetic fields. We have studied the competition between the quantum confinement and applied magnetic field, finding that in this type of heterostructure the geometrical confinement and Al concentration determine the behavior of the electron effective Lande g(parallel to) factor, as compared to the effect of the applied magnetic field. Present theoretical results are in good agreement with experimental reports in the limiting geometry of a quantum well, and with previous theoretical findings in the limiting case of a quantum well wire

Journal of Physics-Condensed Matter 21[45]. 455302. 2009.

P244-09 "Radial Plasma Dynamic in Sequential Pinches"

Kayama, M. E., Clemente, R. A., Honda, R. Y., and Dobrowolsky, M. S.

Plasma dynamic and confinement characteristics were investigated with magnetic probes in a theta pinch operating with oscillatory current waveform and hydrogen gas at pressure between 45 and 150 mtorr. Current-sheath implosion was evident after the third half cycle until sixth half cycle when the external current has practically decayed. Each cycle starts with a trapped reversed magnetic field residual from the previous half cycle. Probe-signal fluctuations due to radial hydromagnetic oscillations were also observed. A modified snowplow model including an initial bias field and a flux-loss term gives a reasonable description of the experimental results for plasma radial dynamic and internal trapped field. Typical equilibrium-density profiles are of a hollow type with maximum density around one-third of the discharge-tube radius. Estimations from these profiles show small variation of temperature and density among half cycles in discharges at low pressure. At high-pressure regime, the temperature strongly drops in subsequent half cycles, while the density increases

Ieee Transactions on Plasma Science 37[11], 2186-2190. 2009.

P245-09 "Splitting of critical energies in the n=0 Landau level of graphene"

Pereira, A. L. C.

The lifting of the degeneracy of states from the graphene n = 0 Landau level (LL) is investigated through a non-interacting tight-binding model with random hoppings. A disorder-driven splitting of two bands and of two critical energies is observed by means of density of states and participation ratio calculations. The analysis of the probability densities of the states within the n = 0 LL provides some insights into the interplay of lattice and disorder effects on the splitting process. An uneven spatial distribution of the wavefunction amplitudes between the two graphene sublattices is found for the states in between the two split peaks. It is shown that as the splitting is increased (linear increasing with disorder and square root increasing with magnetic field), the two split levels also get increasingly broadened, in such a way that the proportion of overlapped states remains approximately constant for a wide range of disorder or magnetic field variation

New Journal of Physics 11. 095019. 2009.

P246-09 "Stabilization of antiferromagnetism in CeFe2 alloys: the effects of chemical and hydrostatic pressure"

Haldar, A., Suresh, K. G., Nigam, A. K., Coelho, A. A., and Gama, S.

Effects of Al, Mn and Sb dopings in CeFe2 and the effect of applied pressure have been investigated. Al doping gives rise to the FM-AFM transition and a reduction in the magnetic moment and T-C values, clearly indicating the growth of the AFM component. Mn and Sb dopings only cause a reduction in the T-C value. It is found that, in general, external pressure enhances the antiferromagnetism in both the pure and the doped alloys. Enhancement of the Ce 4f-Fe 3d hybridization as a result of doping and with the external pressure may be the reason for the stabilization of antiferromagnetism in these alloys

Journal of Physics-Condensed Matter 21[49]. 496003. 2009.

P247-09 "Study of the magnetic and calorimetric properties of (U1-xRx)Cu5Al (R = La and Y)"

da Silva, L. M., dos Reis, R. D., Gandra, F. G., dos Santos, A. O., and Cardoso, L. P.

We have investigated the magnetic and thermodynamic properties of the (U1-x)Cu5Al (R = La and Y) series. The results show a quick decrease of T-N for both La and Y substitutions. For the Y series with concentration between 0.3 <= x <= 0.4, the temperature dependence of the specific heat and magnetic susceptibility below 10 K are consistent with a non-Fermi-liquid regime. (C) 2009 Elsevier B.V. All rights reserved

Physica B-Condensed Matter 404[19], 3176-3178. 2009.

P248-09 "Tantalum based coated substrates for controlling the diameter of carbon nanotubes"

Bouchet-Fabre, B., Djomkam, A. F., Delmas, M., Jin, C., Antonin, O., Hugon, M. C., Mayne-L'Hermite, M. F., Alvarez, F., and Minea, T.

The diameter of carbon nanotubes deposited on TaN coated silicon substrates by catalytic chemical vapor deposition strongly depends on the N/Ta ratio in the coating. The coating characteristics are tailored by controlling the deposition parameters in a plasma reactive sputtering process. Photoelectron emission spectroscopy and X-ray diffraction of the coatings show the formation of a composite material. The presence of multi-wall nanotubes is confirmed by transmission electron microscopy. The results show that the structure of the TAN coating modifies the catalyst (Fe) effect changing the kinetics of the nanotube growth. (c) 2009 Elsevier Ltd. All rights reserved

Carbon 47[15], 3424-3426. 2009.

P249-09 "Texture analysis of computed tomography images of acute ischemic stroke patients"

Oliveira, M. S., Fernandes, P. T., Avelar, W. M., Santos, S. L. M., Castellano, G., and Li, L. M.

Computed tomography (CT) images are routinely used to assess ischemic brain stroke in the acute phase. They can provide important clues about whether to treat the patient by thrombolysis with tissue plasminogen activator. However, in the acute phase, the lesions may be difficult to detect in the images using standard visual analysis. The objective of the present study was to determine if texture analysis techniques applied to CT images of stroke patients could differentiate between normal tissue and affected areas that usually go unperceived under visual analysis. We performed a pilot study in which texture analysis, based on the gray level co-occurrence matrix, was applied to the CT brain images of 5 patients and of 5 control subjects and the results were compared by discriminant analysis. Thirteen regions of interest, regarding areas that may be potentially affected by ischemic stroke, were selected for calculation of texture parameters. All regions of interest for all subjects were classified as lesional or non-lesional tissue by an expert neuroradiologist. Visual assessment of the discriminant analysis graphs showed differences in the values of texture parameters between patients and controls, and also between texture parameters for lesional and non-lesional tissue of the patients. This suggests that texture analysis can indeed be a useful tool to help neurologists in the early assessment of ischemic stroke and quantification of the extent of the affected areas

Brazilian Journal of Medical and Biological Research 42[11], 1076-1079. 2009.

P250-09 "The g-value of Er3+ doped unfilled skutterudite CoSb3 (T-h) reveals the existence of an additional sixth order term in the crystal field Hamiltonian"

Vargas, J. M., Garcia, F. A., Rettori, C., Garcia, D. J., Sales, B., Schlottmann, P., and Oseroff, S. B.

Electron spin resonance (ESR) experiments have been carried out in single crystals of the unfilled skutterudite CoSb3 doped with Er ions. The X- (9.5 GHz) and Q- (34.4 GHz) band spectra obtained at low temperature (4-20 K) shown a temperature independent g-value of 6.21(5). This g-value can only be explained with the addition of a second sixth order B-6(1)(O-6(2) - O-6(6)) term to the usual cubic crystal field Hamiltonian. The ESR of Er3+ show the typical temperature dependence of the line-shape and line-width expected for insulating host. (C) 2009 Elsevier B.V. All rights reserved

Physica B-Condensed Matter 404[19], 3035-3037. 2009.

P251-09 "The role of cationic disorder on the magnetic properties of double perovskites (Ca, Sr)(2-x)LaxFeIrO6"

Bufaical, L., Ferreira, L. M., Lora-Serrano, R., Pagliuso, P. G., Caytuero, A., and Baggio-Saitovich, E.

We have synthesized polycrystalline samples of the series of double-perovskite (DP) type structure (Ca, Sr)(2-x)LaxFeIrO6. Their structural and magnetic properties were investigated by experiments of X-ray powder diffraction, magnetic susceptibility and electrical resistivity. Both series crystallize in a monoclinic structure, space group P2(1)/n (rather than in the triclinic I (1) over bar), with a significant degree of Fe/Ir cationic disorder. Interestingly, our results indicate a change in the nature of the microscopic magnetic interaction induced by La doping, where the system seems to evolve from antiferromagnetic in the extremities of the series, x = 0.0 and 2.0, to ferrimagnetic for intermediate regions of the series. In this work we focus on the comparison of the physical properties of two representative compounds of these families, Ca1.2La0.8FeIrO6 and Sr1.2La0.8FeIrO6, which exhibit the higher magnetization within their series. For the Ca-based sample the disorder is around similar to 34% while was found to be roughly similar to 22% for the Sr2-xLaxFeIrO6 compound. (c) 2009 Elsevier B.V. All rights reserved

Physica B-Condensed Matter 404[19], 3285-3288. 2009.

P252-09 "The spin dynamics of molecular magnets beyond Kubo's linear response theory"

Dartora, C. A., Cabrera, G. G., and Nobrega, K. Z.

The description of quantum dynamics of nanomagnets is a central issue in most applications proposed for those systems. In this paper, we put forward a modified perturbation approach to study the spin dynamics of a molecular magnet in the presence of time-dependent magnetic fields. The non-perturbed Hamiltonian H-0, which defines the interaction picture, may be time-dependent proviso it can be diagonalized at all times by the same basis of states. We probe the method using a simple model Hamiltonian, that contains the important anisotropy terms relevant for Fe-8 molecular clusters, and solve as an example the case with the smallest non trivial spin value (S=1). Our modified perturbation approach converges rapidly to the exact solution, goes beyond the Kubo linear response theory, and is well defined even at resonance. Temperature effects in the spin dynamics are taken into account in the context of the density matrix

Brazilian Journal of Physics 39[3], 587-591. 2009.

P253-09 "Thermal behavior of hard-axis magnetization in noninteracting particles with uniaxial anisotropy"

Ilievski, F., Cuchillo, A., Nunes, W., Knobel, M., Ross, C. A., and Vargas, P.

Experimental evidence is presented to support predictions made by an analytical model describing the temperature-dependent behavior of an assembly of noninteracting magnetic nanoparticles with uniaxial anisotropy under an external field. When the applied field is smaller than the anisotropy field of the particles and is oriented perpendicular to the easy axis, a maximum of the magnetization occurs at finite temperature. The theory shows good agreement with measurements of an array of CoCrPt nanoislands with uniaxial anisotropy. Deviations are discussed taking into account the thermal dependencies of the saturation magnetization and the anisotropy of the magnetic material

Applied Physics Letters 95[20]. 202503. 2009.

P254-09 "Tuning the bottleneck effect in Ag metallic host doped with magnetic Gd and non-magnetic Sb ions"

Vargas, J. M., Oseroff, S. B., and Rettori, C.

The Ag metallic host doped with Gd and Sb is an excellent model system to study the bottleneck effect associated to the conduction-electron (c-e) spin-flip scattering mechanism. Electron spin resonance of Gd3+ in both, Ag-(Gd doped)- and Ag-(Gd and Sb doped)-systems, reveal the presence of bottleneck which can be tuned by the amount of Gd and Sb impurities. The increase of the Gd concentration leads to a c-e spin-flip relaxation rate to the magnetic Gd3+ ions larger than that to the lattice, favoring the bottleneck regime. Whereas the effect of the non-magnetic impurities (Sb ions) is to increase, via spin-orbit scattering, the spin-flip relaxation rate of the c-e to the lattice, weakening the bottleneck regime.

Physica B-Condensed Matter 404[18], 2723-2725. 2009.

Abstracta

Instituto de Física
Diretor: Prof. Dr. Julio Cesar Hadler Neto
Universidade Estadual de Campinas - UNICAMP
Cidade Universitária C.P. 6165
CEP: 13081-970 - Campinas - SP - Brasil
e-mail: secdir@ifi.unicamp.br
Fone: 0XX 19 3521-5300

Publicação

Biblioteca do Instituto de Física Gleb Wataghin
http://webbif.ifi.unicamp.br
Diretora Técnica: Sandra Maria Carlos Cartaxo

Elaboração
Antonela Carvalho Ribeiro
antonela@ifi.unicamp.br

Projeto Gráfico
ÍgneaDesign

Impressão
Gráfica Central - Unicamp